J. Plasma Physics (1998), *vol.* 60, *part* 3, *pp.* 529–539. Printed in the United Kingdom

© 1998 Cambridge University Press

Rayleigh–Bénard convection and pattern formation in magnetohydrodynamics

RENU BAJAJ and S. K. MALIK

Department of Mathematics, Panjab University, Chandigarh 160014, India

(Received 19 September 1997 and in revised form 4 November 1997)

A nonlinear thermal instability in a layer of electrically conducting fluid in the presence of a magnetic field is discussed. Steady-state bifurcation results in the formation of patterns: rolls, squares and hexagons. The stability of various patterns is also investigated. It is found that in the absence of a magnetic field only rolls are stable, but when the magnetic field strength exceeds a certain finite value, squares and hexagons also become stable.

1. Introduction

Convection in horizontal layers of fluid is often accompanied by a cellular pattern of motions (Chandrasekhar 1961; Busse 1967; Koshmieder 1992). The study of Rayleigh–Bénard convection has left a deep imprint on the development of the theory of pattern formation in systems driven away from equilibrium. Gor'kov (1957), Malkus and Veronis (1958) and Schluter *et al.* (1965) have developed the weakly nonlinear theory of convection. The Landau equation representing the evolution of the amplitudes of the convective motion at supercriticality for Boussinesq fluids was obtained by Segal (1969) and Newell and Whitehead (1969). The amplitude of instability was found to be proportional to $(R-R_C)^{1/2}$, where R is the Rayleigh number and R_C is its critical value for the onset of instability. This result has been verified experimentally by Dubois and Bergé (1978), who found rolls to be stable. At high Rayleigh numbers, moderately supercritical convection results in time-dependent flow (see Clever and Busse 1974).

The investigations of Palm (1960), Koshmieder (1966), Segel and Stuart (1962) and Palm *et al.* (1967) revealed that a hexagonal pattern can also exist under supercritical conditions, while hysteresis is possible for subcritical values for a non-Boussinesq fluid. Jenkins (1987) developed a weakly nonlinear theory of convection in a fluid with temperature-dependent viscosity, and reported the existence of square cells. Fauve and Libchaber (1984) performed experiments on convection in mercury. They found that the onset of oscillatory instability depends sensitively on the value of the Rayleigh number and on the Prandtl number of the fluid. A strong magnetic field applied across an electrically conducting fluid has a significant effect on thermal instability. The effect of an applied magnetic field on the onset of thermal instability in electrically conducting fluids is considered by Chandrasekhar (1961). Nakagawa (1957) experimentally studied thermal convection in mercury in the presence of a magnetic field. A magnetic field of strength up to 1.3 T was applied in the direction normal to the fluid. For sufficiently large values of the Chandrasekhar

https://doi.org/10.1017/S0022377898006989 Published online by Cambridge University Press

number Q, the magnetic field aligned the roll axes and suppressed the instability occurring critically. From a large number of streak photographs of cell patterns that developed on the top surface at instability, it was found that the basic cell pattern was hexagonal.

In Rayleigh–Bénard convection in a conducting fluid, in the presence of a magnetic field, instability can occur in two ways:

(i) via steady-state bifurcation, resulting in the appearance of various patterns whose stability depends upon the physical parameters governing the system;

(ii) via Hopf bifurcation, resulting in oscillatory motion.

In this paper, we theoretically study the stability of various steady-state patterns in convection in a horizontal layer of an electrically conducting fluid in the presence of a vertical magnetic field. We use group-theoretical methods and equivariant bifurcation theory (Golubitsky *et al.* 1984, 1988; Golubitsky and Schaeffer 1985) to discuss the relative stability of patterns – rolls, squares and hexagons.

In Sec. 2, we formulate the nonlinear convection problem as a bifurcation problem. The linear analysis in Sect. 3 gives the critical value of the Rayleigh number for the onset of instability as steady-state bifurcation and Hopf bifurcation. This depends upon the Prandtl numbers σ and P_1 and the Chandrasekhar number Q. We assume the set of physical parameters of the system to be such that only steady-state bifurcation occurs and oscillatory instability is avoided. As the Rayleigh number R is increased beyond the critical value, steady-state bifurcation results in the appearance of patterns. The nonlinear solutions for rolls, squares and hexagons are found in Sec. 4. The stability of patterns is discussed in Sec. 5.

2. Formulation

Consider an infinite horizontal layer of electrically conducting fluid. An adverse temperature gradient is maintained across the layer by heating from below. A uniform vertical magnetic field $\mathbf{H}$ is applied across the fluid layer. The fluid is assumed to satisfy the Boussinesq approximation. The system of equations governing the physical system is

$$\frac{\partial \mathbf{v}}{\partial t} + (\mathbf{v}\cdot\boldsymbol{\nabla})\,\mathbf{v} - \frac{\mu}{4\pi\rho}(\mathbf{H}\cdot\boldsymbol{\nabla})\,\mathbf{H} = -\boldsymbol{\nabla}\left(\frac{P}{\rho} + \frac{\mu H^2}{8\pi\rho}\right) + \mathbf{g}\left(1 + \frac{\delta\rho}{\rho}\right) + \nu\nabla^2\mathbf{v}, \tag{1}$$

where ρ, P, μ, ν and $\mathbf{v} = (u, v, w)$ are the density, pressure, magnetic permeability, coefficient of viscosity and velocity field respectively. The magnetic field $\mathbf{H}$ satisfies

$$\frac{\partial \mathbf{H}}{\partial t} + (\mathbf{v}\cdot\boldsymbol{\nabla})\,\mathbf{H} = (\mathbf{H}\cdot\boldsymbol{\nabla})\,\mathbf{v} + \eta\nabla^2\mathbf{H}, \tag{2}$$

$$\boldsymbol{\nabla}\cdot\mathbf{H} = 0, \tag{3}$$

where η is the resistivity of the fluid. The energy equation satisfied by the temperature is

$$\frac{\partial T}{\partial t} + (\mathbf{v}\cdot\boldsymbol{\nabla})\,T = k_T\nabla^2 T, \tag{4}$$

https://doi.org/10.1017/S0022377898006989 Published online by Cambridge University Press

where T is the temperature and k_T is the thermal conductivity of the fluid. Also, the fluid satisfies the usual equation of continuity

$$\boldsymbol{\nabla}\cdot\mathbf{v}=0. \tag{5}$$

The equation of state is

$$\rho=\rho_0[1-\alpha_T(T-T_0)], \tag{6}$$

where T_0 is the equilibrium temperature and α_T is the thermal coefficient.

Equations (1)–(6) are rendered dimensionless by using characteristic values of length, velocity, temperature as l, $k_T l^{-1}$ and γl respectively, where $\gamma=-\partial T/\partial z$ is the temperature gradient. We obtain

$$\frac{\partial\mathbf{v}}{\partial t}+(\mathbf{v}\cdot\boldsymbol{\nabla})\,\mathbf{v}-Q\sigma P_1(\mathbf{H}\cdot\boldsymbol{\nabla})\,\mathbf{H}-H_0\frac{\mu}{4\pi\rho}(\mathbf{H}_0\cdot\boldsymbol{\nabla})\,\mathbf{H}=-\boldsymbol{\nabla}P'-R\sigma T\hat{\mathbf{z}}, \tag{7}$$

$$\frac{\partial\mathbf{H}}{\partial t}+(\mathbf{v}\cdot\boldsymbol{\nabla})\,\mathbf{H}=(\mathbf{H}\cdot\boldsymbol{\nabla})\,\mathbf{v}+P_1\nabla^2\mathbf{H}, \tag{8}$$

$$\frac{\partial T}{\partial t}+(\mathbf{v}\cdot\boldsymbol{\nabla})\,T=\nabla^2T, \tag{9}$$

$$\boldsymbol{\nabla}\cdot\mathbf{H}=0, \tag{10}$$

$$\boldsymbol{\nabla}\cdot\mathbf{v}=0, \tag{11}$$

where $Q=\mu H_0^2l^2/4\pi\rho_0\nu\eta$ is the Chandersekhar number, $R=g\alpha_T\gamma l^4/\nu k_T$ is the Rayleigh number, and $\sigma=\nu/k_T$ and $P_1=\eta/k_T$ are the Prandtl numbers.

The equations governing the departures of temperature (T'), magnetic field (H') and pressure from their equilibrium values are

$$\begin{aligned}-\frac{\partial}{\partial t}\nabla^2u+\sigma\nabla^4u+\left[-\left(\frac{\partial^2}{\partial y^2}+\frac{\partial^2}{\partial z^2}\right)(\mathbf{v}\cdot\boldsymbol{\nabla})\,u+\frac{\partial^2}{\partial x\,\partial y}(\mathbf{v}\cdot\boldsymbol{\nabla})\,v+\frac{\partial^2}{\partial x\,\partial z}(\mathbf{v}\cdot\boldsymbol{\nabla})\,w\right]\\ =R\sigma\frac{\partial^2T'}{\partial x\,\partial z}+Q\sigma P_1\left[-\frac{\partial}{\partial z}\nabla^2h_x'-\left(\frac{\partial^2}{\partial y^2}+\frac{\partial^2}{\partial z^2}\right)(\mathbf{h}'\cdot\boldsymbol{\nabla})\,h_x'+\frac{\partial^2}{\partial x\,\partial y}(\mathbf{h}'\cdot\boldsymbol{\nabla})\,h_y'\right.\\ \left.+\frac{\partial^2}{\partial x\,\partial z}(\mathbf{h}'\cdot\boldsymbol{\nabla})\,h_z'\right],\end{aligned} \tag{12}$$

$$\begin{aligned}-\frac{\partial}{\partial t}\nabla^2v+\sigma\nabla^4v+\left[-\left(\frac{\partial^2}{\partial x^2}+\frac{\partial^2}{\partial z^2}\right)(\mathbf{v}\cdot\boldsymbol{\nabla})\,v+\frac{\partial^2}{\partial x\,\partial y}(\mathbf{v}\cdot\boldsymbol{\nabla})\,u+\frac{\partial^2}{\partial y\,\partial z}(\mathbf{v}\cdot\boldsymbol{\nabla})\,w\right]\\ =R\sigma\frac{\partial^2T'}{\partial y\,\partial z}+Q\sigma P_1\left[-\frac{\partial}{\partial z}\nabla^2h_y'-\left(\frac{\partial^2}{\partial x^2}+\frac{\partial^2}{\partial z^2}\right)(\mathbf{h}'\cdot\boldsymbol{\nabla})\,h_y'+\frac{\partial^2}{\partial x\,\partial y}(\mathbf{h}'\cdot\boldsymbol{\nabla})\,h_x'\right.\\ \left.+\frac{\partial^2}{\partial y\,\partial z}(\mathbf{h}'\cdot\boldsymbol{\nabla})\,h_z'\right],\end{aligned} \tag{13}$$

https://doi.org/10.1017/S0022377898006989 Published online by Cambridge University Press

$$-\frac{\partial}{\partial t}\nabla^2 w+\sigma\nabla^4 w+\left[-\left(\frac{\partial^2}{\partial x^2}+\frac{\partial^2}{\partial y^2}\right)(\mathbf{v}\cdot\boldsymbol{\nabla})\,w+\frac{\partial^2}{\partial x\,\partial z}(\mathbf{v}\cdot\boldsymbol{\nabla})\,u+\frac{\partial^2}{\partial y\,\partial z}(\mathbf{v}\cdot\boldsymbol{\nabla})\,v\right]$$
$$=R\sigma\left(\frac{\partial^2 T'}{\partial x^2}+\frac{\partial^2 T'}{\partial y^2}\right)+Q\sigma P_1\left[-\frac{\partial}{\partial z}\nabla^2 h'_z-\left(\frac{\partial^2}{\partial x^2}+\frac{\partial^2}{\partial y^2}\right)(\mathbf{h}'\cdot\boldsymbol{\nabla})\,h'_z\right.$$
$$\left.+\frac{\partial^2}{\partial x\,\partial z}(\mathbf{h}'\cdot\boldsymbol{\nabla})\,h'_x+\frac{\partial^2}{\partial y\,\partial z}(\mathbf{h}'\cdot\boldsymbol{\nabla})\,h'_y\right], \tag{14}$$

$$\frac{\partial\mathbf{h}'}{\partial t}+(\mathbf{v}\cdot\boldsymbol{\nabla})\,\mathbf{h}'=(\mathbf{h}'\cdot\boldsymbol{\nabla})\,\mathbf{v}+P_1\nabla^2\mathbf{h}'+\frac{\partial w}{\partial z}, \tag{15}$$

$$\frac{\partial T'}{\partial t}+(\mathbf{v}\cdot\boldsymbol{\nabla})\,T'=\nabla^2 T'+w. \tag{16}$$

The boundary conditions at the horizontal boundaries $z=0,1$ are

$$w=\frac{\partial^2 w}{\partial z^2}=T'=h'_z=0. \tag{17}$$

The normal component of the magnetic field is continuous across the boundary. The basic equations and the boundary conditions (12)–(17) governing the problem are equivariant under the Euclidean group E(2) and also with respect to reflection in the midplane. Therefore, the symmetry group of the problem is $\mathrm{E}(2)\times\mathbb{Z}_2$.

3. Linear theory

The system of equations (12)–(17) has trivial conduction solution $(\mathbf{v},T,H)=(0,0,0)$. As the Rayleigh number R, which is proportional to the temperature gradient, is increased beyond a critical value, instability sets in and convection starts. The linear dispersion relation is found to be

$$\omega^3(\pi^2+k^2)-\omega^2(\sigma+P_1+1)\,(\pi^2+k^2)^2+w[-(\pi^2+k^2)^3\,(\sigma P_1+\sigma+P_1)$$
$$+R\sigma k^2-Q\sigma P_1\,\pi^2(\pi^2+k^2)]+\sigma P_1(\pi^2+k^2)^4-R\sigma k^2(\pi^2+k^2)\,P_1$$
$$+Q\sigma P_1\,\pi^2(\pi^2+k^2)=0. \tag{18}$$

Bifurcation can occur either as steady-state bifurcation ($\omega=0$) or as Hopf bifurcation ($\mathrm{Re}\,\omega=0$, $\mathrm{Im}\,\omega\neq 0$). The critical values of Rayleigh number for the two types of bifurcation are different, R_{ss} for steady-state bifurcation and R_{Hopf} for Hopf bifurcation:

$$R_{ss}=\frac{(\pi^2+k^2)^3+\pi^2 Q(\pi^2+k^2)}{k^2},\qquad k=k_{CS}, \tag{19}$$

$$R_{\mathrm{Hopf}}=\frac{(\sigma+P_1)\,[(1+P_1)\,(1+\sigma)\,(\pi^2+k^2)^3+Q\sigma P_1\,\pi^2(\pi^2+k^2)]}{\sigma(\sigma+1)\,k^2},\qquad k=k_{CH}. \tag{20}$$

The stability diagrams for steady-state bifurcation and Hopf bifurcation are

https://doi.org/10.1017/S0022377898006989 Published online by Cambridge University Press

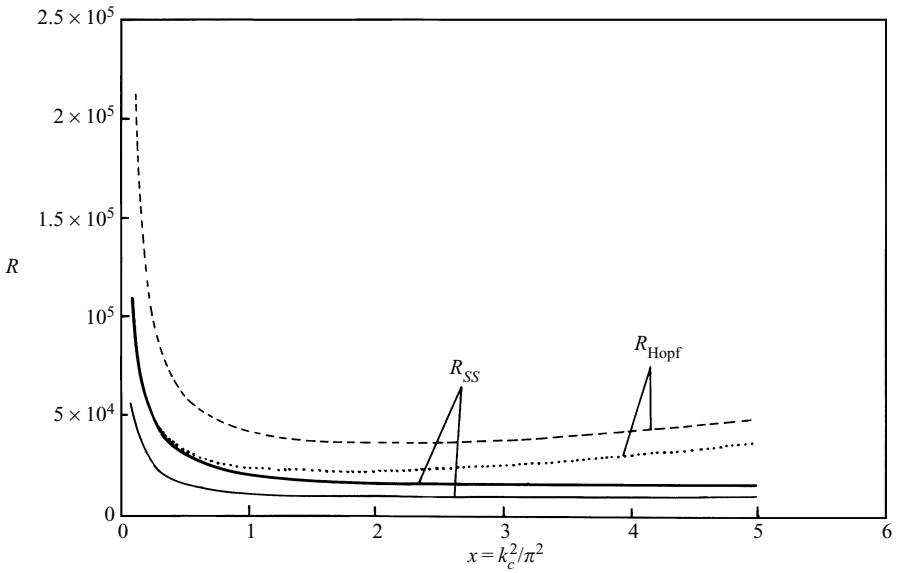


Figure 1. Linear stability diagrams for steady-state bifurcation and Hopf bifurcation: —— and ....., $Q = 500$; ▬ and ———, $Q = 1000$.

shown in Fig. 1. We find that for Hopf bifurcation,

$$(\mathrm{Im}\,\omega)^2 = -(\pi^2+k^2)^2 P_1^2 + \frac{Q\pi^2\sigma P_1(1-P_1)}{1+\sigma}.$$

For $P_1 \geqslant 1$, $(\mathrm{Im}\,\omega)^2 < 0$, which is not possible. Therefore Hopf bifurcation cannot occur for $P_1 \geqslant 1$. Hopf bifurcation results in oscillatory motion. In this paper, we shall study the motion resulting from the steady-state bifurcation. We choose the values of the physical parameter $P_1 \geqslant 1$ so that the instability arises as a result of steady-state bifurcation only.

4. Nonlinear theory

In order to develop the nonlinear analysis, we use group-theoretical methods and equivariant bifurcation theory (Golubitsky *et al.* 1984, 1988; Golubitsky and Schaeffer 1985; Buzano and Golubitsky 1983; Silber and Knobloch 1988; Guckenheimer and Holmes 1983). The stability of the fluid is characterized by the Rayleigh number R. The bifurcation parameter λ is defined by

$$\lambda = \frac{R-R_{SS}}{R_{SS}}.$$

In general, the linearized equation has an infinite-dimensional kernel at every point about the critical state. Therefore, Liapunov–Schmidt reduction cannot be performed. We consider a finite-dimensional kernel by making use of experimental observations of spatially periodic rolls, squares and hexagons.

The vertical velocity w is taken as a doubly periodic scalar real valued function on $\mathbb{R}^2$, with periods $\mathbf{e}_1$ and $\mathbf{e}_2$. $\mathscr{L}$ is the lattice generated by $\mathbf{e}_1$ and $\mathbf{e}_2$. The translational symmetry of the doubly periodic function w is identified with

https://doi.org/10.1017/S0022377898006989 Published online by Cambridge University Press

$\mathbb{T}^2 = \mathbb{R}^2/\mathscr{L}$. The rotational part of E(2) has discrete symmetries D_4 for a square pattern and D_6 for a hexagonal pattern. Thus the symmetry group of the square lattice is $\Gamma_S = D_4 \times \mathbb{T}^2$ and that of the hexagonal lattice is $\Gamma_H = D_6 \times \mathbb{T}^2$. Rolls and squares lie on a square lattice, whereas rolls and hexagons lie on a hexagonal lattice. The steady-state equation for the vertical velocity w is

$$L_0(w) = \lambda L_1(w) + N_1(\mathbf{v}, \mathbf{v}) + R_{SS} N_2(\mathbf{v}, T') + N_3(\mathbf{v}, \mathbf{h}') + N_4(\mathbf{h}', \mathbf{h}'), \tag{21}$$

where

$$L_0(w) = \sigma \nabla^6 w - R_{SS}\, \sigma \nabla_1^2 w - Q\sigma \nabla^2 D^2 w, \tag{22}$$

$$\nabla^2 = \frac{\partial^2}{\partial x^2} + \frac{\partial^2}{\partial y^2} + \frac{\partial^2}{\partial z^2}, \qquad D = \frac{\partial}{\partial z}, \qquad \nabla_1^2 = \frac{\partial^2}{\partial x^2} + \frac{\partial^2}{\partial y^2}, \tag{23}$$

$$L_1(w) = \sigma \nabla_1^2 w, \tag{24}$$

$$N_1(\mathbf{v}, \mathbf{v}) = \left[\left(\frac{\partial^2}{\partial x^2} + \frac{\partial^2}{\partial y^2} \right) (\mathbf{v} \cdot \nabla)\, w - \frac{\partial^2}{\partial x\, \partial z} (\mathbf{v} \cdot \boldsymbol{\nabla})\, u - \frac{\partial^2}{\partial y\, \partial z} (\mathbf{v} \cdot \boldsymbol{\nabla})\, v \right], \tag{25}$$

$$N_2(\mathbf{v}, T') = -\sigma \left[\left(\frac{\partial^2}{\partial x^2} + \frac{\partial^2}{\partial y^2} \right) (\mathbf{v} \cdot \boldsymbol{\nabla})\, T' \right], \tag{26}$$

$$N_3(\mathbf{v}, \mathbf{h}') = -Q\sigma \nabla^2 \left[\frac{\partial}{\partial z} \left((\mathbf{v} \cdot \boldsymbol{\nabla})\, h_z' - (\mathbf{h}' \cdot \boldsymbol{\nabla})\, w \right) \right], \tag{27}$$

$$N_4(\mathbf{h}', \mathbf{h}') = Q\sigma P_1 \nabla^2 \left[-\left(\frac{\partial^2}{\partial x^2} + \frac{\partial^2}{\partial y^2} \right) (\mathbf{h}' \cdot \boldsymbol{\nabla})\, h_z' + \frac{\partial^2}{\partial x\, \partial z} (\mathbf{h}' \cdot \boldsymbol{\nabla})\, h_x' + \frac{\partial^2}{\partial y\, \partial z} (\mathbf{h}' \cdot \boldsymbol{\nabla})\, h_y' \right]. \tag{28}$$

To find the bifurcation solution of these equations in the neighbourhod of R_{SS}, the various physical quantities w, T', h', u, v and λ are expressed in the form

$$\Phi = A\Phi_1 + A^2\Phi_1 + A^3\Phi_3 + \mathscr{O}(A^4). \tag{29}$$

Also,

$$R = R_{SS}(1 + R_1 A + R_2 A^2 + \cdots), \tag{30}$$

where A denotes the pattern amplitude.

A third-order analysis is carried out to find the amplitudes of rolls, squares and hexagons.

At lowest order in A, (21) admits the solutions

$$\text{(R)}: \quad w_1^R = \exp(ik_c x) \sin \pi z + \text{c.c.}; \tag{31}$$

$$\text{(S)}: \quad w_1^S = [\exp(ik_c x) + \exp(ik_c y)] \sin \pi z + \text{c.c.}; \tag{32}$$

$$\text{(H)}: \quad w_1^H = \{\exp(ik_c x) + \exp[ik_c(-x + \sqrt{3}y)/2] + \exp[ik_C(x + \sqrt{3}y)/2]\} \sin \pi z + \text{c.c.} \tag{33}$$

Proceeding to second order, (21) yields

$$L_0(w_2) = R_1 L_1(w_1) + N_1(\mathbf{V}_1, \mathbf{V}_1) + R_{SS} N_2(\mathbf{V}_1, T_1') + N_3(\mathbf{V}_1, \mathbf{h}_1') + N_4(\mathbf{h}_1', \mathbf{h}_1'). \tag{34}$$

Where R_1 is the coefficient of the first-order term in the expansion (29) for λ. With a view to obtaining uniformly valid solutions, we require that the

https://doi.org/10.1017/S0022377898006989 Published online by Cambridge University Press

solutions w_2 of this equation be spatially periodic. This condition implies that all terms on the right-hand side of (34) lying in the kernel of L_0 must vanish. Since none of the nonlinear terms in (34) lie in the kernel of L_0, we require that

$$R_1^R = R_1^S = R_1^H = 0. \tag{35}$$

This condition yields the solutions

$$(\mathrm{R}): \quad w_2^R = 0; \tag{36}$$

$$(\mathrm{S}): \quad w_2^S = \alpha f(x,y)\sin 2\pi z, \tag{37}$$

where

$$f(x,y) = \exp[ik_c(x+y)] + \exp[ik_c(x-y)] + \text{c.c.}, \tag{38}$$

and α is found to be

$$\alpha = 2\pi\left[\frac{(\pi^2+k_C^2)^2}{\sigma} - \frac{R_{SS}k_C^2}{2k_C^2+4\pi^2} + \frac{Q\pi^2}{P_1}\right](\pi^2+k_C^2)^{-1} \times\left[-(4\pi^2+2k_C^2)^2 + \frac{2R_{SS}k_C^2}{(2k_C^2+4\pi^2)} - 4Q\pi^2\right]^{-1}; \tag{39}$$

$$(\mathrm{H}): \quad w_2^H = [\beta_1 g_1(x,y) + \beta_2 g_2(x,y)]\sin 2\pi z, \tag{40}$$

$$g_1(x,y) = \exp(i\theta_1) + \exp(i\theta_2) + \exp(i\theta_3) + \text{c.c.}, \tag{41}$$

$$g_2(x,y) = \exp[i(2\theta_1+\theta_2)] + \exp[i(\theta_1+2\theta_2)] + \exp[i(\theta_1-\theta_2)] + \text{c.c.}, \tag{42}$$

and

$$\theta_1 = x, \qquad \theta_2 = (-x+\sqrt{3}y)/2, \qquad \theta_3 = \theta_1+\theta_2,$$

where

$$\beta_1 = \frac{3\pi}{2}\left[\frac{(\pi^2+k_C^2)^2}{\sigma} - \frac{R_{SS}k_C^2}{k_C^2+4\pi^2} + \frac{Q\pi^2}{P_1}\right](\pi^2+k_C^2)^{-1} \times\left[-(4\pi^2+k_C^2)^2 + \frac{2R_{SS}k_C^2}{(k_C^2+4\pi^2)} - 4Q\pi^2\right]^{-1}, \tag{43}$$

$$\beta_2 = \frac{3\pi}{2}\left[\frac{(\pi^2+k_C^2)^2}{\sigma} - \frac{R_{SS}k_C^2}{3k_C^2+4\pi^2} + \frac{Q\pi^2}{P_1}\right](\pi^2+k_C^2)^{-1} \times\left[-(4\pi^2+3k_C^2)^2 + \frac{2R_{SS}k_C^2}{(3k_C^2+4\pi^2)} - 4Q\pi^2\right]^{-1}. \tag{44}$$

At third order, (21) is

$$\begin{aligned} L_0(w_3) = {} & R_2 L_1(w_1) + N_1(\mathbf{V}_1, \mathbf{V}_2) + N_1(\mathbf{V}_2, \mathbf{V}_1) \\ & + R_{SS}[N_2(\mathbf{V}_1, T_2') + N_2(\mathbf{V}_2, T_1')] \\ & + N_3(\mathbf{V}_1, \mathbf{h}_2') + N_3(\mathbf{V}_2, \mathbf{h}_1') \\ & + N_4(\mathbf{h}_1', \mathbf{h}_2') + N_4(\mathbf{h}_2', \mathbf{h}_1'). \end{aligned} \tag{45}$$

Where R_2 is the coefficient of the first-order term in the expansion (29) for λ. On proceeding as in the second-order case, the solvability condition determines R_2

https://doi.org/10.1017/S0022377898006989 Published online by Cambridge University Press

for rolls, squares and hexagons:

$$R_2^R = \frac{(\pi^2+k_C^2)^2+\pi^2 Q}{2k_C^2}; \tag{46}$$

$$R_2^S = \frac{\pi\alpha}{k_C^2}\left[-\frac{(\pi^2+k_C^2)^2}{\sigma}+\frac{Q\pi^2}{P_1}-\frac{R_{SS}\,k_C^2}{2k_C^2+4\pi^2}+\frac{4\pi^2(\pi^2+k_C^2)\,Q}{(4\pi^2+2k_C^2)\,P_1}\right] + \frac{R_{SS}}{k_C^2+\pi^2}\left(1+\frac{\pi^2}{2k_C^2+4\pi^2)}\right), \tag{47}$$

where α is as given in (39);

$$R_2^H = \frac{3\pi\beta_1}{k_c^2}\left[-\frac{(\pi^2+k_C^2)^2}{2\sigma}+\frac{Q\pi^2}{2P_1}-\frac{R_{SS}\,k_C^2}{(2k_C^2+4\pi^2)} + \frac{2\pi^2(\pi^2+k_C^2)\,Q}{(4\pi^2+2k_C^2)\,P_1}-\frac{\pi^4 Q}{3(4\pi^2+2k_C^2)\,P_1}\right]+\frac{\pi\beta_2}{k_c^2}\left[-\frac{(\pi^2+k_C^2)^2}{2\sigma}+\frac{Q\pi^2}{2P_1} - \frac{R_{SS}\,k_C^2}{2(3k_C^2+4\pi^2)}+\frac{2\pi^2(\pi^2+k_C^2)\,Q}{(4\pi^2+3k_C^2)\,P_1}-\frac{\pi^4 Q}{3(4\pi^2+2k_C^2)\,P_1}\right] + \frac{R_{SS}}{2(k_C^2+\pi^2)}\left[3+\frac{\pi^2}{2(3k_C^2+4\pi^2)}+\frac{9\pi^2}{2(k_C^2+4\pi^2)}\right], \tag{48}$$

where β_1 and β_2 are given in (43) and (44) respectively. The pattern amplitude is given by

$$A = (\lambda/R_2)^{1/2}, \tag{49}$$

where $R_2 = R_2^R = R_2^S = R_2^H$ for rolls, squares and hexagons respectively are given in (46), (47) and (48).

5. Stability analysis

The finite-dimensional normal form of the equation governing the amplitude for the square lattice is (Golubitsky *et al.* 1988)

$$n(x_1, x_2, \lambda) = (\epsilon_0\,\lambda + mN)\begin{pmatrix}x_1\\x_2\end{pmatrix}+\epsilon_1\,\delta\begin{pmatrix}x_1\\-x_2\end{pmatrix}, \qquad m = 0, \epsilon_1, \tag{50}$$

where

$$N = x_1^2+x_2^2, \qquad \delta = x_2^2-x_1^2.$$

The stability of rolls and squares is determined by the parameters ϵ_0, ϵ_1 and m. The bifurcation analysis of (50) yields stable supercritical rolls for $\epsilon_1 = -1$ and $m < -1$, and stable supercritical squares for $\epsilon_1 = 1$ and $m < 0$.

For the system under consideration, since the trivial solution is stable subcritically,

$$\epsilon_0 = 1, \qquad \epsilon_1 = \mathrm{sgn}(2R_2^R - R_2^S), \qquad m = \frac{\epsilon_1 R_2^S}{R_2^S - 2R_2^S},$$

where R_2^R and R_2^S are given in (46) and (47) respectively. Degeneracies occur for $m = 0$, ϵ_1 and $2R_2^R - R_2^S = 0$. It has been found numerically that $R_2^R > 0$

https://doi.org/10.1017/S0022377898006989 Published online by Cambridge University Press

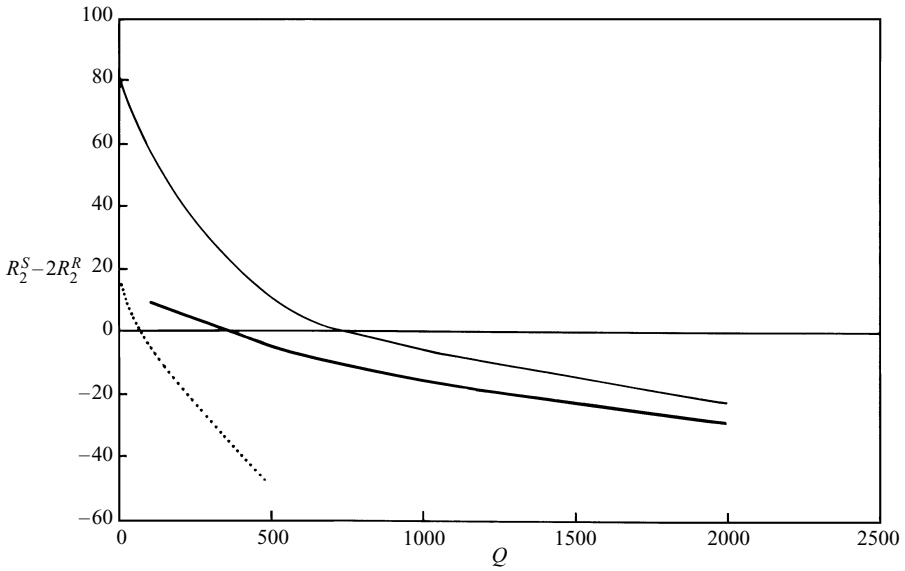


Figure 2. Variation of $R_2^S-2R_2^R$ with Q. The point where the curve intersects the Q axis give the value of Q_0. Squares are stable for $Q > Q_0$ and rolls are stable for $Q < Q_0$. ——, $\sigma = 0.3$, $P_1 = 1.5$; ▬, $\sigma = 1$, $P_1 = 1.5$; ....., $\sigma = 1$, $P_1 = 1$.

and $R_2^S > 0$ for all possible values of the physical parameters σ, P_1 and Q. $2R_2^R-R_2^S = 0$ for $Q = Q_0$ for $\sigma = 0.3$ and 1 and $P_1 = 1.5$ and 1, which is shown in Fig. 2. Stable rolls are obtained for $Q < Q_0$, whereas stable square patterns occur for $Q > Q_0$.

The universal unfolding for the normal form of the vector field with hexagonal symmetry (Buzano and Golubitsky 1983) is

$$\left.\begin{aligned} &\dot{z}_i = z_i(\lambda + a\sigma_i + u_i) + cq\bar{z}_j\,\bar{z}_k + \mathcal{O}(z^5, \lambda^2 z, \lambda z^3), \\ &i,j,k = 1,2,3; \qquad i = j = k, \\ &a+1 \neq 0, \qquad 2a+1 \neq 0, \qquad 3a+1 \neq 0, \qquad c \neq \pm 1, \\ &\sigma_1 = u_1+u_2+u_3, \qquad \sigma_2 = u_1u_2+u_2u_3+u_3u_1, \qquad \sigma_3 = u_1u_2u_3, \\ &q = z_1z_2z_3+\bar{z}_1\bar{z}_2\bar{z}_3, \qquad u_i = z_i\bar{z}_i. \end{aligned}\right\} \tag{52}$$

The coefficient a for our system is found to be

$$a = (R_2^R-R_2^H)\,(R_2^H-3R_2^R)^{-1}, \tag{53}$$

where R_2^R and R_2^H have already been determined as in (46) and (48) respectively. The nontrivial roll solutions are stable for $a < -1$ i.e. $R_2^R > 0$ and $R_2^H-3R_2^R > 0$, whereas hexagons are stable for $R_2^H-3R_2^R < 0$ and $R_2^H > 0$.

We have found numerically that $R_2^H > 0$ and $R_2^R > 0$ for all values of σ, P_1 and Q. A plot of $R_2^H-3R_2^R$ against Q is shown in Fig. 3. The value of Q where the curve intersects the Q axis is Q_1. $R_2^H-3R_2^R < 0$ for $Q > Q_1$, and $R_2^H-3R_2^R > 0$ for $Q < Q_1$. Therefore, stable hexagons are obtained for $Q > Q_1$ and stable rolls occur for $Q < Q_1$. Hysteresis is absent here owing to the presence of $\mathbb{Z}_2$ symmetry in the system of equations.

https://doi.org/10.1017/S0022377898006989 Published online by Cambridge University Press

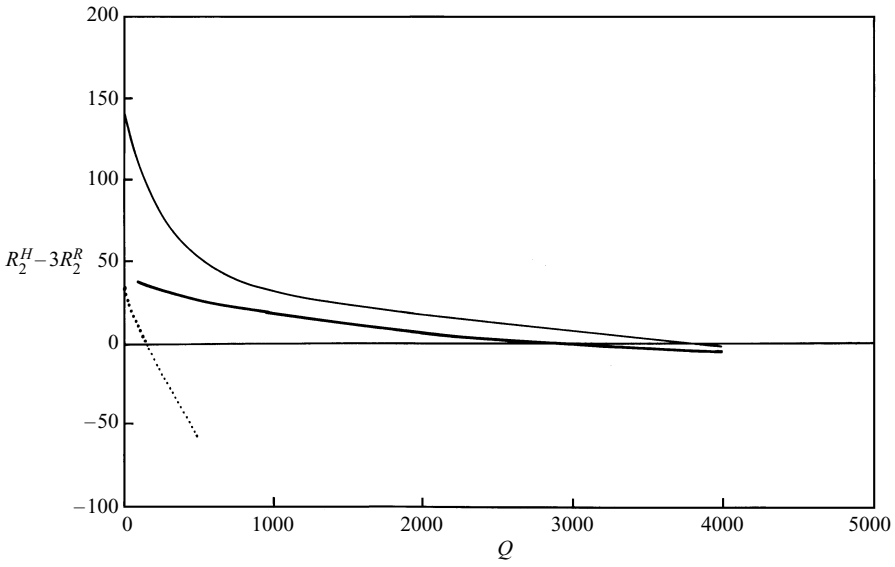


Figure 3. Variation of $R_2^H - 3R_2^R$ with Q. The point where the curve intersects the Q axis gives the value of Q_1. Hexagons are stable for $Q > Q_1$ and rolls are stable for $Q < Q_1$. ——, $\sigma = 0.3$, $P_1 = 1.5$; ▬▬, $\sigma = 1$, $P_1 = 1.5$; ....., $\sigma = 1$, $P_1 = 1$.

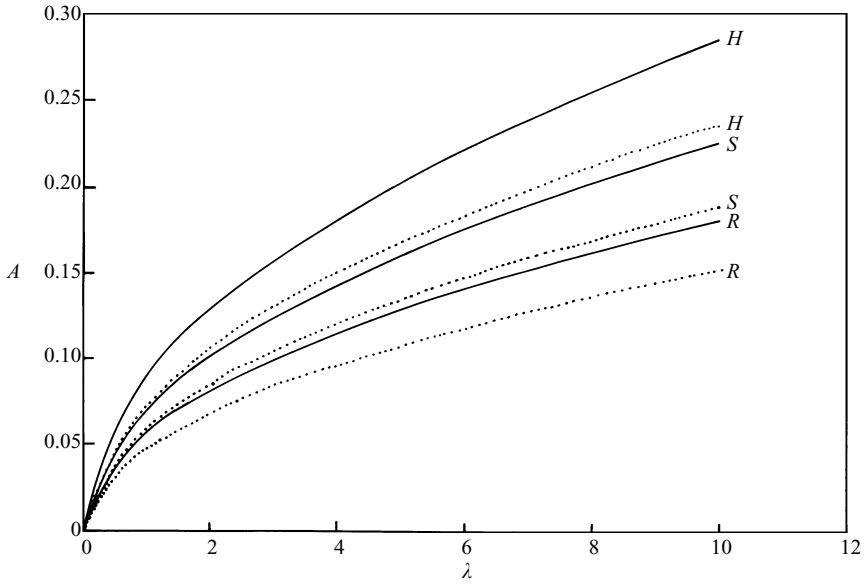


Figure 4. Amplitudes of rolls, squares and hexagons in the (λ, A) plane for $\sigma = 1$ and $P_1 = 1$: ....., $Q = 500$; ——, $Q = 1000$.

For a fixed value of the Prandtl number $P_1 = 1.5$, an increase in the value of the Prandtl number σ decreases the values of Q_0 and Q_1 beyond which squares and hexagons respectively are stable. On the other hand, for a fixed value of σ, an increase in P_1 increases the values of Q_0 and Q_1.

The amplitudes of the patterns are shown in Fig. 4. It has been observed that

https://doi.org/10.1017/S0022377898006989 Published online by Cambridge University Press

the amplitudes of rolls, squares and hexagons decrease with increasing value of the parameter Q.

We note that for $Q = 0$, in the absence of a magnetic field, only rolls are stable on both square and hexagonal lattices. By applying a magnetic field of sufficient intensity that the Chandrasekhar number $Q > Q_0$, Q_1, we can obtain stable square and hexagonal patterns respectively. We also observe numerically that $Q_0 < Q_1$. For $Q_0 < Q < Q_1$, squares are found to be stable and hexagons unstable, whereas for $Q > Q_1$, both squares and hexagons are stable. We cannot find the relative stability of squares and hexagons using this analysis, since there exists no two-dimensional lattice with both D_4 and D_6 as subgroups. This is a shortcoming of the analysis. However, we shall find the relative instability between squares and hexagons using a multiple-scale method in a forthcoming paper, on which work is in progress.

Acknowledgement

The authors are grateful to the Council of Scientific and Industrial Research, India for financial support.

References

Busse, F. H. 1967 *J. Math. Phys.* **46**, 140–149.

Buzano, E. and Golubitsky, M. 1983 *Phil. Trans. R. Soc. Lond.* **A308**, 249–276.

Chandrasekhar, S. 1961 *Hydrodynamic and Hydromagnetic Stability*. Oxford University Press.

Clever, R. M. and Busse, F. H. 1974 *J. Fluid Mech.* **65**, 625–645.

Dubois, M. and Bergé, P. 1978 *J. Fluid Mech.* **85**, 641–654.

Fauve, S. and Libchaber, A. 1984 *Chaos and Order in Nature* (ed. H. Haken), pp. 25–35. Springer-Verlag, Berlin.

Golubitsky, M., Swift, J. W. and Knobloch, E. 1984 *Physica* **D10**, 249–276.

Golubitsky, M. and Schaeffer, D. G. 1985 *Singularities and Groups in Bifurcation Theory*, Vol. I. Springer-Verlag, New York.

Golubitsky, M., Stewart, I. N. and Schaeffer, D. G. 1988 *Singularities and Groups in Bifurcation Theory*, Vol. II. Springer-Verlag, New York.

Gor'kov, L. P. 1957 *Zh. Eksp. Teor. Fiz.* **33**, 402–407.

Guckenheimer, J. and Holmes, P. 1983 *Nonlinear Oscillations, Dynamical Systems and Bifurcation of Vector Fields*. Springer-Verlag, New York.

Jenkins, D. R. 1987 *J. Fluid Mech.* **178**, 491–506.

Koschmieder, E. L. 1992 *Bénard Cells and Taylor Vortices*. Cambridge University Press.

Koschmieder, E. L. 1966 *Beitr. phys. Atmos.* **39**, 1–11.

Malkus, W. V. R. and Veronis, G. 1958 *J. Fluid Mech.* **4**, 225–260.

Newell, A. C. and Whitehead, J. A. 1969 *J. Fluid Mech.* **38**, 279–303.

Nakagawa, Y. 1957 *Proc. R. Soc. Lond.* **A240**, 108–113.

Palm, E. 1960 *J. Fluid Mech.* **8**, 183–192.

Palm, E., Elmgren, T. and Gjevik, B. 1967 *J. Fluid Mech.* **30**, 651–661.

Schlüter, A., Lortz, D. and Busse, F. 1965 *J. Fluid Mech.* **23**, 129–144.

Segel, L. A. 1969 *J. Fluid Mech.* **38**, 203–224.

Segel, L. A. and Stuart, J. T. 1962 *J. Fluid Mech.* **13**, 289–306.

Silber, M. and Knobloch, E. 1988 *Phys. Rev.* **A38**, 1468–1477.

https://doi.org/10.1017/S0022377898006989 Published online by Cambridge University Press